JACS
JOURNAL OF THE AMERICAN CHEMICAL SOCIETY

ARTICLE

pubs.acs.org/JACS

Probing Ionophore Selectivity in Argon-Tagged Hydrated Alkali Metal Ion−Crown Ether Systems

Jason D. Rodriguez and James M. Lisy*

Department of Chemistry, University of Illinois, Urbana—Champaign, 600 South Mathews Avenue, Urbana, Illinois 61801, United States

Supporting Information

ABSTRACT: Crown ethers are an important family of compounds that are closely related to naturally occurring ionophores. Thus, crown ethers are useful in modeling the size-selective behavior of ionophores. Using a combination of infrared predissociation spectroscopy and density functional theory calculations, we have investigated M^+(18-crown-6 ether)$(H_2O)_{1-4}$ Ar complexes, where M = Li, Na, K, Rb and Cs in the gas phase. The argon-tagging technique was used to lower the internal energies (effective temperatures ∼100 K), yielding well-resolved spectra in the OH stretching region for systems containing up to three waters. Spectral changes were monitored as both the size of the ion and degree of hydration were varied. While there is not a particular spectroscopic signature of gas-phase selectivity reported in this work, the unique role that K^+ plays in the systems studied, as a "bridge" between the smaller and larger alkali metal ions, is consistent with the well-known special affinity for K^+ by 18-crown-6 ether in the aqueous phase.

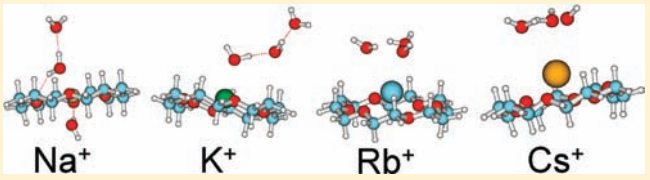

1. INTRODUCTION

Since their discovery by Pedersen[1−3] in the 1960s, crown ethers have become the most widely used model system in the study of ionophore size-selectivity. One of the most common crown ethers, 18-crown-6 ether (18c6) is known to be a K^+-selective ionophore[4] in aqueous solution. Extensive condensed-phase work[5−7] suggested that this special affinity was due to a "best-fit" match[4] between the size of K^+ and the 18c6 cavity. While this was the prevailing reasoning for two decades, subsequent gas-phase work by Dearden[8,9] and Brodbelt[10,11] seemed to contradict the "best-fit" model and found that the smaller alkali metal ions, Li^+ and Na^+, were bound to 18c6 more tightly than K^+ when studying the unsolvated M^+(18c6) systems in the gas phase. The initial discrepancy between condensed-phase and gas-phase studies seemed to be due to the effect of hydration. Indeed, later experimental[12,13] work by Armentrout and co-workers as well as theoretical[14] efforts by Feller, revealed the crucial role that hydration plays in these systems; as the solvation environment evolves, the prevailing non-covalent interactions also evolve. Furthermore, it is the competition and balance of these non-covalent interactions that determine ionophore selectivity.[13]

The combination of spectroscopic and theoretical techniques to probe crown ether systems has been an active topic by our group[15−18] and others[19−25] over the past few years. The complexes, $M^+(18c6)(H_2O)_{1-4}$, previously reported by evaporative cooling of water,[17] contained broad, unresolved features with as few as two waters present, precluding in-depth analysis of the larger hydrated M^+(18c6) systems. This report considers the non-covalent interactions in $M^+(18c6)(H_2O)_{1-4}$Ar systems as a function of ion size and degree of hydration as determined by infrared predissociation (IRPD) spectroscopy in the OH stretching region and density functional theory (DFT) calculations. Since the species reported here are stabilized by evaporative cooling and tagging with argon (Ar-tagging),[26] they have low internal energies (and corresponding effective temperatures of ∼100 K) which yield well-resolved spectra in most cases. This allows us to track changes and interpret spectral trends more easily than the analogous warm (untagged) clusters formed by evaporative cooling of H_2O.[17] In addition, the combination of low internal energy and low binding energy of Ar facilitates the trapping of higher energy structural conformers, a process that we have documented in previous publications for several systems.[15,27−31]

2. METHODS

2.1. Experimental Section. Since our experimental apparatus has been described in detail elsewhere, only a brief overview is presented here. Argon carrier gas seeded with a small amount of H_2O (∼0.02%) is passed trough a heated cell (80−100 °C) containing solid 18c6. The resulting mixture is forced through a 180° conical nozzle with typical backing pressures of ∼500−600 Torr. The gas mixture is allowed to fully expand, forming Ar-rich clusters before being impacted at 90° by ions ejected from a custom-made ion gun. The nascent cluster ions stabilize primarily via the evaporation of Ar. The cluster ion beam is then skimmed and guided through a differentially pumped intermediate chamber by a combination of an octapole ion guide and electrostatic lenses to the detector chamber, which contains the triple quadrupole mass spectrometer portion of our apparatus. In the first quadrupole, the parent cluster ions of interest are mass selected. While in the second

Received: August 24, 2010
Published: June 15, 2011

dx.doi.org/10.1021/ja107383c | J. Am. Chem. Soc. 2011, 133, 11136–11146

(ion guiding) quadrupole, the parent cluster ions interact with the output of a tunable laser (LaserVision OPO/A pumped by a 10 Hz Continuum Surelite II Nd:YAG), which is scanned from 3100 to 3800 cm^{-1} to cover the entire OH stretching region. The third quadrupole is used to mass analyze fragments resulting from photodissociation following single-photon absorption in the second quadrupole. The fragments are then detected and an IRPD spectrum is acquired as a function of laser frequency. Typically, the third quadrupole is set to a mass associated with the loss of the most labile ligand after photoexcitation, which usually corresponds to the loss of Ar. Absolute frequency calibration (± 3 cm^{-1}) is achieved by simultaneously acquiring the photoacoustic spectrum of atmospheric H_2O.

2.2. Calculations. We have performed DFT calculations to assist in the characterization of our experimental results. Starting geometries were generated in Spartan 02[32] and then fully optimized using the tight-convergence criteria (root-mean-square force threshold of 3×10^{-5} hartrees/bohr) in Gaussian 03.[33] Harmonic vibrational frequency calculations were then performed on the fully optimized geometries. All reported geometries and frequency calculations were carried out at the B3LYP/6-31+G** level of theory. The LANL2DZ ECP[34−36] basis set augmented by Glendening polarization functions[37] was used for Rb and Cs atoms. Starting geometries were initially generated by having the ion approach the neutral $(18c6)(H_2O)_{1-4}$ complex from multiple trajectories to ensure that all possible configurations were considered. Whenever a unique configuration was found for one of the ions, we attempted to find the same configuration for the others. In many cases, some configurations that are observed for the larger ions were not observed for the smaller, and vice versa. The main factor responsible for this behavior was the size of the ion, which limited the types of conformers that were observed for each ion. Although it is possible that some conformers were missed, we believe that this approach has located the major conformers as most of the spectral features observed experimentally can be found among the computational conformers. All visual representations of optimized geometries were acquired using Molden.[38] The output of the harmonic vibrational frequency calculations were transformed into simulated IR spectra in SWizard[39] with 15 cm^{-1} full-width-half-maximum Lorentzian line shapes. In the comparison between the experimental and simulated IR spectra, two frequency scaling factors were applied to the harmonic frequencies: 0.954 for non-hydrogen-bonded OH vibrations and 0.966 for hydrogen-bonded OH vibrations. The use of multiple scaling factors is becoming increasingly common in comparing experimental and computational results, and the value used in this study for the hydrogen-bonded vibrations is very consistent with previously reported values.[40] Despite the use of scaling factors we estimate typical errors in our simulated IR spectra to be ~10−30 cm^{-1}. Thermodynamic analysis was conducted using Thermo.pl[41] based on the harmonic vibrational frequency calculations and all energies reported have been zero-point energy (ZPE) corrected (using the unscaled vibrational frequencies). Calculations with and without Ar conducted on the smaller systems indicated that Ar did not have a significant impact on the optimized geometries or calculated vibrational frequencies (± 2 cm^{-1}) and intensities (± 10 km/mol) for these complexes, a result consistent with previous studies.[42] Including Ar in the calculations may, however, slightly affect the relative energy ordering (~1−5 kJ/mol) at the level of theory used. In light of these findings, all comparative calculations reported were performed without Ar. We include additional information on this topic in the Supporting Information.

3. RESULTS AND DISCUSSION

3.1. $M^+(18c6)(H_2O)_1Ar$ Complexes. The IRPD spectra of the $M^+(18c6)(H_2O)_1Ar$ complexes in the OH stretching region are shown in Figure 1. The spectra were acquired by monitoring the loss of Ar. The existence of a prominent OH feature near

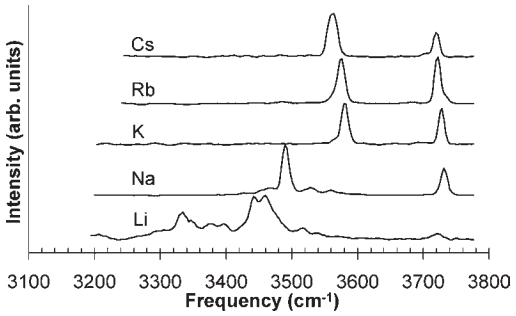

Figure 1. Experimental IRPD spectral summary of $M^+(18c6)(H_2O)_1Ar$ complexes in the OH stretching region monitoring the loss of Ar.

3720 cm^{-1} for all the ions (except Li) and features below 3600 cm^{-1} indicate that H_2O is significantly perturbed by the presence of 18c6. For the sake of comparison we note that the OH symmetric and asymmetric stretching frequencies of $M^+(H_2O)_1Ar$ are above 3600 cm^{-1} for all of the alkali ions.[43−45] In the $M^+(18c6)(H_2O)_1Ar$ complexes, the 18c6···H_2O hydrogen-bonding interaction is significant even when only one H_2O is present. As has been noted in earlier reports,[46] OH stretches below 3600 cm^{-1} are associated with hydrogen bond formation between the OH group and a proton acceptor which, in the case of the $n = 1$ complexes, is the 18c6 oxygen. The band at 3720 cm^{-1} is due to the other OH group, called the free OH, which does not participate in hydrogen bonding. There is a noticeable shift in the spectral trend that occurs from Na^+ to K^+. The spectra of the smaller ions, Li^+ and Na^+, exhibit strong hydrogen-bonding interactions that shift the OH stretching vibrations to frequencies below 3500 cm^{-1}. Strong hydrogen-bonding interactions are possible since Li^+ and Na^+ are small enough to fit inside the 18c6 cavity, while also binding the lone H_2O closely to 18c6. This is an excellent case where potentially competing 18c6···M^+ and 18c6···H_2O non-covalent interactions work *cooperatively* to form stronger hydrogen bonds. A new trend begins with K^+ and continues to Cs^+, where one OH stretching feature for each of these ions occurs just below 3600 cm^{-1}.

The fully optimized DFT geometries for $n = 1$ complexes are shown in Figure 2. Since the effective temperature of cluster ions formed by Ar evaporation in our apparatus was previously reported[27] to be in the range of ~50−150 K, we report relative free energies at 0 and 100 K. In Figure 2 and throughout the study, the conformers are ordered according to their energies at 100 K and labeled alphabetically. Only one stable conformer was found for Li^+, Li1A. This conformer features the H_2O in a bidentate hydrogen-bonding orientation with two 18c6 oxygen atoms while also interacting with Li^+. The top view is given in Figure 2 to emphasize the differences in the location of the ion as ionic size increases from Li^+ to K^+. This bidentate orientation of H_2O gives rise to the broad feature at ~3450 cm^{-1} in the experimental spectrum shown in Figure 1. While there is the possibility that other conformers not found in our analysis are also populated in the experiment, the lack of a prominent free OH stretch at ~3700 cm^{-1} provides further support for a bidentate configuration.

One of the two stable conformers shown in Figure 2 for the $Na^+(18c6)(H_2O)_1$ system also features a bidentate orientation (Na1B). This conformer is 35.9 kJ/mol higher in energy at 100 K than the lower-energy structure, Na1A. As shown in Table 1, the

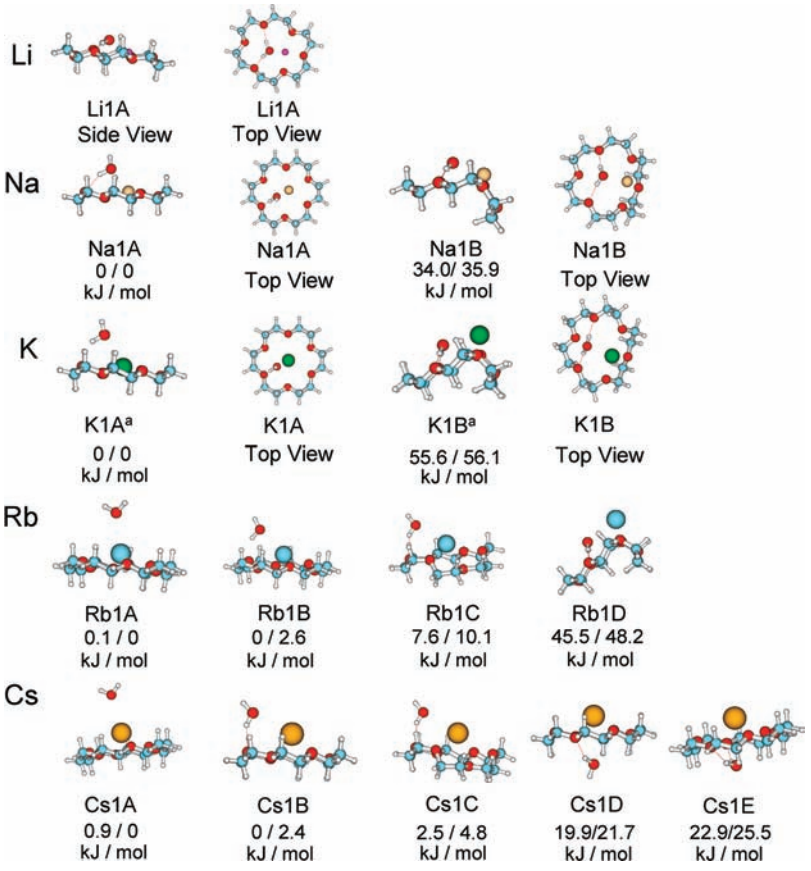

Figure 2. Fully optimized geometries of candidate $M^+(18c6)(H_2O)_1$ conformers at the B3LYP/6-31+G** level of theory (Ar atoms not included). The relative Gibbs free energies (ΔG in kJ/mol) are also given at 0 K/100 K. The conformers are ordered according to their 100 K energies. For Li^+, Na^+, and K^+ a top view is shown to illustrate the ion binding inside the 18c6 cavity. [a]The $K^+(18c6)(H_2O)_1$ conformers and energies were previously reported in ref 15.

predicted frequencies for Na1A are in strong agreement with the peak positions observed in the experiment. Conformer Na1B does not appear to be present based in Table 1. Conformer Na1A features the H_2O lying above the $Na^+(18c6)$ complex while interacting with both the ion and 18c6. The sharp feature 3490 cm^{-1} is due to the 18c6···H_2O hydrogen-bonding interaction. The Na1A conformer was also predicted for the untagged $Na^+(18c6)(H_2O)_1$ complex.[17] The $K^+(18c6)(H_2O)_1Ar$ system has already been reported,[15] and the predicted vibrational frequencies of conformer K1A match well with the experimental frequencies, as shown in Table 1. The feature present at 3580 cm^{-1} is due to the 18c6···H_2O hydrogen-bonding interaction. While K1A and Na1A are the same type of conformers, Na1A displays a more linear O−H···O bond angle (Na, 155°; K, 140°) and longer O−H bond length (Na, 0.982 Å; K, 0.976 Å) which both signal the formation of a stronger hydrogen bond and a shift to lower frequency of the OH stretch in the Na^+ conformer compared to the K^+ conformer.

The spectra for both $Rb^+(18c6)(H_2O)_1Ar$ and $Cs^+(18c6)(H_2O)_1Ar$ continue the trends established with K^+. The larger ionic diameter[47] of these ions, 2.94 and 3.34 Å for Rb^+ and Cs^+, respectively, compared to that 18c6 cavity size of 2.6−3.2 Å makes it energetically unfavorable for the ions to lie in the interior of the 18c6 cavity. This impacts the way that the H_2O binds in the Rb^+ and Cs^+ complexes. In the case of Cs^+, stable opposite-side binding is predicted for some of the higher energy conformers. As shown in Figure 3 and Table 1, there are multiple conformers for both Rb^+ and Cs^+ that may give rise to the spectral signature shown in Figure 1. It is interesting to note that the lowest energy conformers (Rb1A and Cs1A) do not appear to be observed in the experimental spectra, while some of the other conformers lying higher in relative energy clearly are. This requires some examination into the factors that may be at play in these systems. First, the energy difference between the two lowest-lying conformers for Rb^+ and Cs^+ is less than 3 kJ/mol. As noted earlier and discussed in the Supporting Information, the effect of Ar on the relative binding energies is in the 1−5 kJ/mol range. So the correct ordering of these conformers bearing Ar is somewhat uncertain. Second, although the DFT calculations performed are unable to pinpoint the location of the Ar (see Supporting Information), the configurations most likely to bind Ar would maximize the interaction between Ar and the cluster ion. This would likely involve direct Ar···M^+ contact (∼5 kJ/mol) and thus would favor geometries where the Ar has clear access to M^+. As can be seen in Figure 2, this can be easily done for conformers Rb1B and Cs1B, which are within the uncertainty of the energy ordering. In Figure 3 and Table 1, the computed spectra and frequencies of these conformers are consistent with the experimental results. The other conformers: Rb1C, Cs1C and Cs1D are also possible, but are somewhat higher in relative energy and, except for Cs1C, are outside the uncertainty in energy. It is also noteworthy that the calculations for the $M^+(18c6)(H_2O)_1Ar$ systems, as shown in Table 1, capture both the sharp change in the frequency position of the 18c6···H_2O interaction in going

Table 1. Experimentally Observed and Calculated OH Stretching Frequencies (in cm^{-1}) for $M^+(18c6)(H_2O)_1Ar$ Complexes Along with Their Assignments[a]

exptl cluster[b]	exptl frequency[c]	OH stretching assignment	conformer	calcd frequency	OH stretching assignment
$Na^+(18c6)(H_2O)_1Ar$	3732	free	Na1A	3727	free
	3490	18c6···H_2OH-bond		3484	18c6···H_2OH-bond
			Na1B	*3581*	*bidentate H-bond*
				3525	*bidentate H-bond*
$K^+(18c6)(H_2O)_1Ar$	3727	free	K1A	3720	free
	3580	18c6···H_2OH-bond		3584	18c6···H_2O H-bond
			K1B[d]	*3593*	*bidentate H-bond*
				3529	*bidentate H-bond*
			Rb1A	*3731*	*asymmetric*
				3632	*symmetric*
$Rb^+(18c6)(H_2O)_1Ar$	3722	free	Rb1B	3719	free
	3574	18c6···H_2OH-bond		3565	18c6···H_2O H-bond
			Rb1C	3719	free
				3564	18c6···H_2O H-bond
			Rb1	*3619*	*bidentate H-bond*
				3554	*bidentate H-bond*
			Cs1A	*3730*	*asymmetric*
				3631	*symmetric*
$Cs^+(18c6)(H_2O)_1Ar$	3720	free	Cs1B	3716	free
	3562	18c6···H_2OH-bond		3538	18c6···H_2O H-bond
			Cs1C	3716	free
				3539	18c6···H_2O H-bond
			Cs1D	3720	free
				3593	18c6···H_2O H-bond
			Cs1E	*3719*	*bidentate H-bond*
				3616	*bidentate H-bond*

[a] Italicized conformers are not believed to be present in the Ar loss experimental spectra. [b] $Li^+(18c6)(H_2O)_1Ar$ not included due to lack of clearly resolved features in Figure 1A. [c] Peak centers (±3 cm^{-1}) based on the experimental spectra shown in Figure 1A. [d] Frequencies based on ref 15.

from Na^+ to K^+ as well as the gradual shift to lower frequency of the 18c6···H_2O interaction from $K^+ \rightarrow Cs^+$. The latter is apparent by comparing conformers K1A, Rb1B, Rb1C, Cs1B, and Cs1C.

As reported in a previous study[15] of the of the $K^+(18c6)(H_2O)_1Ar$ system, we found that Ar-tagging can lead to the trapping of substantially higher energy conformers in our experiment that are not detected in the Ar loss channel. The Ar-rich environment of the neutral clusters favors the formation of neutral binary complexes, where H_2O is bound to 18c6 in a bidentate configuration with both OH groups involved in hydrogen bonds. As the ion approaches the neutral complex, rapid Ar evaporation[27] favors a minimum energy path. If the evaporative cooling process produces a complex with insufficient internal energy to overcome the barrier leading to a lower-energy configuration, this higher energy conformer can then be kinetically trapped. Upon irradiation by an IR photon, these barriers may be overcome. The photon energy and additional energy gained by rearrangement can lead to more extensive fragmentation with the loss of all ligands (Ar + H_2O) to form the highly stable $M^+(18c6)$ complex. For the $M^+(18c6)(H_2O)_1Ar$ systems, this corresponds to monitoring the Ar + H_2O loss channel. The spectra acquired by monitoring this fragmentation channel are shown in Figure 4. The Li^+ spectrum is not included in the loss of Ar + H_2O series since the energy to dissociate Ar + H_2O (~110 kJ/mol) exceeds the energy available from the photon and the cluster ion internal energy. There is no loss-channel dependence noted for the Na^+ spectrum, which has essentially the same spectrum as the one acquired monitoring the Ar loss channel. This clearly indicates that conformer Na1B is not likely to be present in our experiment to an appreciable extent. The K^+, Rb^+, and Cs^+ spectra acquired monitoring the loss of Ar + H_2O are very different than those presented in Figure 1 and indicate the presence of the high-energy conformers in the experiment. The high energy $K^+(18c6)(H_2O)_1Ar$ bidentate structure, K1B, was reported and assigned in an earlier study.[15] The hydrogen-bonded features belonging to the bidentate conformers (K1B and Rb1D) are indicated for K^+ and Rb^+. The Cs^+ spectrum is highly congested, indicating there are many possible conformers that are probed by monitoring the Ar + H_2O loss channel. Additional IRPD spectra acquired monitoring the Ar + H_2O loss channel for the $M^+(18c6)(H_2O)_{2-4}Ar$ systems are contained in the Supporting Information.

3.2. $M^+(18c6)(H_2O)_2Ar$ Complexes. The IRPD spectra of the $M^+(18c6)(H_2O)_2Ar$ complexes acquired monitoring the loss of Ar are shown in Figure 5. With the addition of the second H_2O, there is a significant increase in the number of features in the hydrogen-bonding region, below 3600 cm^{-1}. Like in the $M^+(18c6)(H_2O)_1Ar$ systems, there is a transition in the spectra in going from Na^+ to K^+ for the $M^+(18c6)(H_2O)_2Ar$ complexes. This again indicates that the 18c6···M^+ interaction for the smaller ions is clearly impacting the interactions involving H_2O.

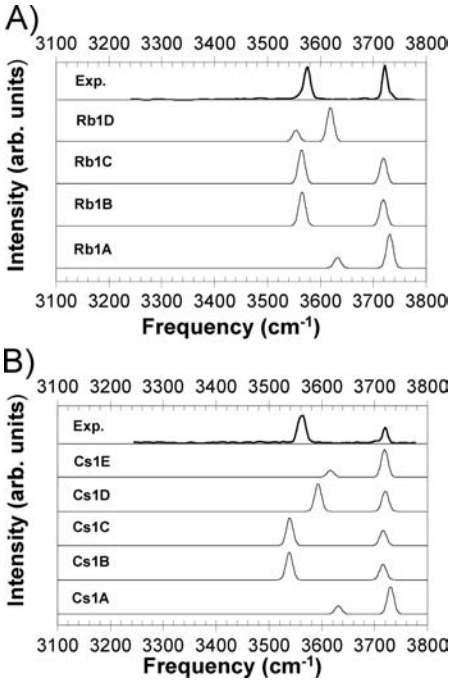

Figure 3. Comparison of experimental IRPD spectra and simulated IR spectra based on the harmonic vibrational frequency calculations for (A) $Rb^+(18c6)(H_2O)_1$ and (B) $Cs^+(18c6)(H_2O)_1$ systems. All of the spectra have been normalized to their maximum intensity and offset for clarity.

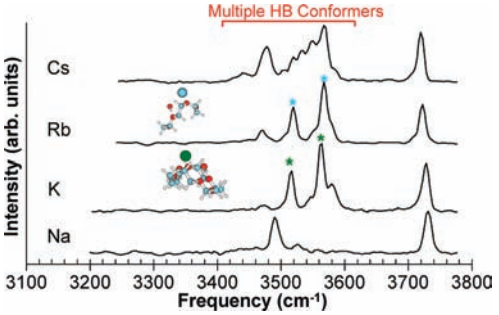

Figure 4. Experimental IRPD spectral summary of $M^+(18c6)(H_2O)_1Ar$ complexes in the OH stretching region monitoring the loss of Ar + H_2O. The signature of the bidentate conformation is noted with asterisks for K^+ and Rb^+.

Both Li^+ and Na^+ spectra have hydrogen-bonding features that are shifted to lower OH stretching frequencies than the larger alkali metal ions. All of the spectra contain a free OH stretch at ~3720 cm^{-1}. The Li^+ spectrum contains a second, higher-frequency feature just above 3750 cm^{-1} and a broad, weaker feature at ~3630 cm^{-1} that indicate the presence of a conformer with a H_2O that is not a proton donor. These features likely correspond to the asymmetric and symmetric stretching vibrations, which appear[48] at 3756 and 3657 cm^{-1}, respectively in gas-phase neutral H_2O, and 3691 and 3631 cm^{-1} in $Li^+(H_2O)_1Ar$.[44] Since there is no clear evidence of these features for any of the other ions, it appears that more extensive hydrogen-bonding is present for the complexes involving the larger alkali metal ions.

To determine the type of hydrogen bonding, whether 18c6···H_2O or H_2O···H_2O, and to assist in the characterization of the

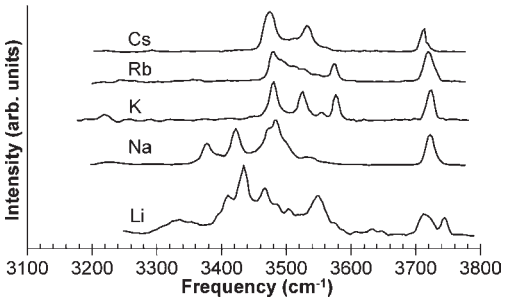

Figure 5. Experimental IRPD spectral summary of $M^+(18c6)$-$(H_2O)_2Ar$ complexes in the OH stretching region monitoring the loss of Ar.

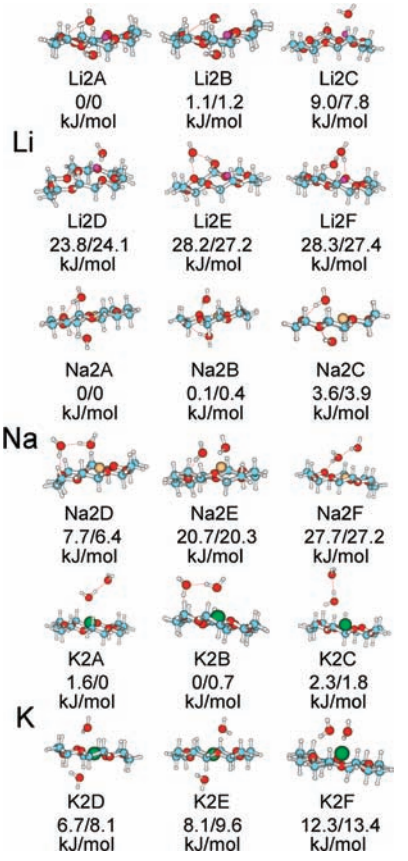

Figure 6. Fully optimized geometries of candidate $M^+(18c6)(H_2O)_2$ conformers at the B3LYP/6-31+G** level of theory (argon atoms not included) for M = Li, Na, and K. The relative Gibbs free energies (ΔG in kJ/mol) are also given at 0 K/100 K. The conformers are ordered according to their 100 K energies.

IRPD spectra in Figure 5, we carried out DFT calculations on the $M^+(18c6)(H_2O)_2$ systems. The optimized geometries for Li^+, Na^+, and K^+ are shown in Figure 6. Due to space considerations we include the low energy conformations for each ion as well as those believed to be present in the experiment. Additional conformers not included in Figure 6 are contained in the Supporting Information. It is interesting to note that both Li^+ and Na^+ have a low-lying "sandwich"-type configuration where a H_2O is on either side of the 18c6-M^+ complex (Li2A and Na2A). This stable configuration is also observed for K^+ but not for

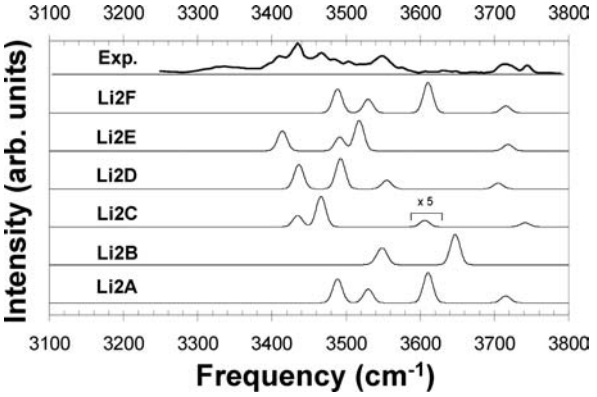

Figure 7. Comparison of experimental IRPD spectra and simulated IR spectra based on the harmonic vibrational frequency calculations for the $Li^+(18c6)(H_2O)_2$ system. All of the spectra have been normalized to their maximum intensity and offset for clarity. The symmetric OH stretching feature in Li2C has also been enhanced (×5).

Rb^+ and Cs^+ at the level of theory used in this work (vide infra). This again underscores the nature of binding for the smaller ions to 18c6 in a way that impacts interactions with H_2O.

The four lowest-energy conformations for the $Li^+(18c6)(H_2O)_2Ar$ system are extensions of the Li1A conformer shown in Figure 2. Conformer Li2A features a sandwich-type orientation, with the ion nestled inside 18c6 and having a H_2O on either side. Conformers Li2C through Li2F have a same-side-type orientation, referring to the ion and all waters lying on the same side of 18c6. This type of configuration causes a sharp rise in the relative energies, indicating that the $Li^+(18c6)(H_2O)_2$ system is most stable in the sandwich-type orientation. In comparing the simulated IR spectra of the six possible conformers with the experiment, shown in Figure 7, it is difficult to eliminate any of the conformers from being present in the experiment based on their simulated IR spectra. Indeed, the number of features in the experimental spectrum strongly suggests multiple conformers are present. Even the presence of higher energy conformers cannot be discounted since trapping of high-energy conformers by Ar-tagging has been well-established for $Li^+(H_2O)_4Ar$.[27,31] One thing that Figure 7 does establish, however, is that the second H_2O in conformer Li2C, which is coordinated to Li^+ and is not participating in a hydrogen bond, is likely responsible for the aforementioned peak just above 3750 cm^{-1} and the area of weaker intensity at ~3630 cm^{-1}, which correspond to the asymmetric and symmetric OH stretches, respectively, of H_2O in the experimental spectrum. The feature at ~3630 cm^{-1} might also have contributions from conformer Li2A and Li2B.

The $Na^+(18c6)(H_2O)_2Ar$ spectrum shown in Figure 5 is much different than the $Na^+(18c6)(H_2O)_1Ar$ spectrum in Figure 1, having a series of prominent hydrogen-bonded OH stretches at 3378, 3422, and 3481 cm^{-1}. There is also a broad feature with weaker intensity at ~3530 cm^{-1}. For Na^+, it is possible for the second H_2O to bind via a number of same-side- and/or sandwich-type configurations as evidenced by the four lowest-energy conformations (in Figure 6) all lying within 6.4 kJ/mol. The three lowest energy conformers are all different versions of the sandwich-type H_2O configuration. While both Na2A and Na2B are isoenergetic and have very similar structures, they do have some differences in their simulated IR spectra, namely a ~25 cm^{-1} shift in the hydrogen-bonded feature. This feature is actually due to the 18c6···H_2O hydrogen-bonding interaction for the waters located above and below 18c6. They appear as only one feature in the simulated spectrum for both conformers because they are nearly identical and their predicted splitting is less than the convolution line width used. Both Na2A and Na2B seem to replicate the weaker feature at 3530 cm^{-1} and the more intense feature at 3481 cm^{-1}, respectively, in the experimental spectrum as seen in Figure 8A. The latter feature is noticeably broader than the other features observed in the experiment and may be due to other conformers also contributing to this feature such as Na2D. The simulated spectrum of Na2C is different than Na2A and Na2B due to the underside H_2O, which gives rise to two new bands predicted to be near 3584 and 3677 cm^{-1}. Since there is clearly no evidence of the latter feature, it is likely that this conformer does not significantly contribute to the experiment. The same-side conformers, Na2D, Na2E and Na2F, all have hydrogen-bonded water networks that may give rise to the lower frequency hydrogen-bonded bands in the 3350−3450 cm^{-1} region. The 3422 and 3378 cm^{-1} features present in the experimental spectrum correlate well with Na2E and Na2F, respectively.

The $Na^+(18c6)(H_2O)_2Ar$ experimental spectrum also provides an excellent opportunity to gauge the temperature dependence on the conformations populated in the experiment. Figure 8B shows the comparison between the spectrum of untagged[17] $Na^+(18c6)(H_2O)_2$, with an effective temperature of about ~298 K, and Ar-tagged $Na^+(18c6)(H_2O)_2Ar$, with an effective temperature of about ~100 K. The two lowest energy conformers, Na2A and Na2B, with sandwich-type structures, accurately reproduce the two experimental features, a hydrogen-bonded OH stretch at 3520 cm^{-1}, and the free OH stretch at 3730 cm^{-1} in the spectrum of the untagged species. The Ar-tagging method has clearly generated additional conformers with more extensive $H_2O\cdots H_2O$ hydrogen-bonding interactions from same-side configurations. This underscores the two (seemingly contradictory) effects of using Ar-tagging: lowering the internal energies and trapping of higher energy conformers when the energy barrier to rearrangement exceeds the Ar-binding energy.[15,27−31]

The six candidate conformations found for the $K^+(18c6)(H_2O)_2$ system are shown in Figure 6. The experimental IRPD spectrum for $K^+(18c6)(H_2O)_2Ar$ along with the simulated IR spectra for each of the candidate conformers are shown in Figure 9A. The most intense hydrogen-bonded OH stretches at 3480 and 3525 cm^{-1} appear to be associated with these three lowest-lying same-side configurations (K2A, K2B, and K2C). These bands arise from the $H_2O\cdots H_2O$ hydrogen-bonding interactions in these configurations. Among these, the presence of K2C in the experiment seems unlikely since there is no appreciable intensity in the 3635 cm^{-1} region. The highest-frequency hydrogen-bonded OH stretch in the experiment at 3576 cm^{-1} is likely due to one or more of the conformers K2D, K2E, and K2F, arising from the 18c6···H_2O hydrogen-bonding interaction. While not in exact quantitative agreement with the experimental frequencies, these calculated bands are adequate to qualitatively explain the hydrogen-bonding region in the experimental spectrum. When we consider the possible influence of Ar, as done for the Rb^+ and Cs^+ systems containing a lone H_2O, K2B, K2D and K2E conformers have configurations which give the Ar access to K^+. This should favor the presence of these conformers in the $K^+(18c6)(H_2O)_2Ar$ spectrum. If one were to construct a composite spectrum from the K2B and K2D (or K2E) spectra, one would have an adequate qualitative representation of the experimental spectrum.

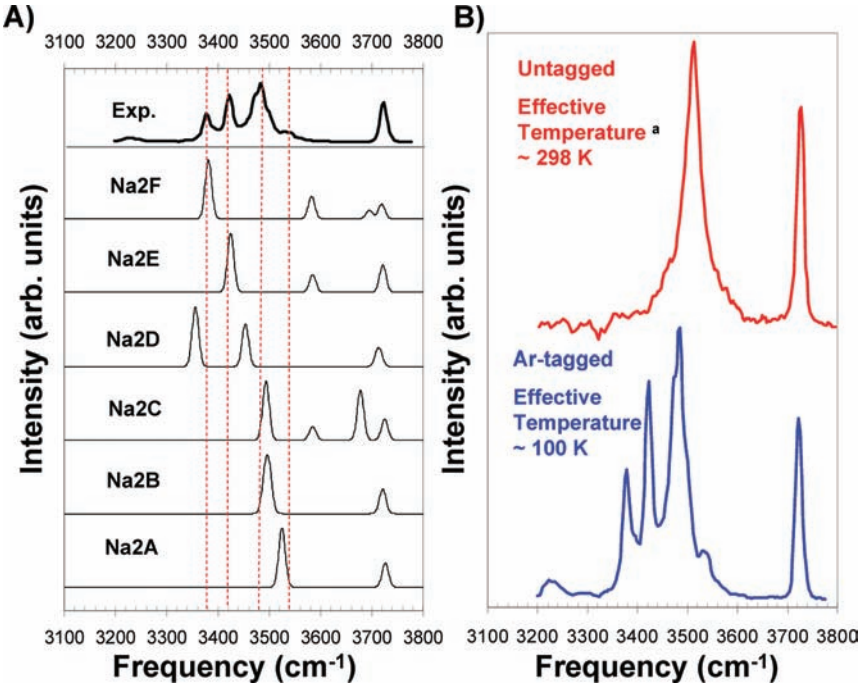

Figure 8. (A) Comparison between experiment and calculations for $Na^+(18c6)(H_2O)_2$. (B) Temperature dependent spectra for $Na^+(18c6)(H_2O)_2$. [a]The untagged spectra have been previously reported ref 17. All of the spectra have been normalized to their maximum intensity and offset for clarity. The red-dotted line in (A) is used to guide the eye and facilitate comparison with the simulated spectra.

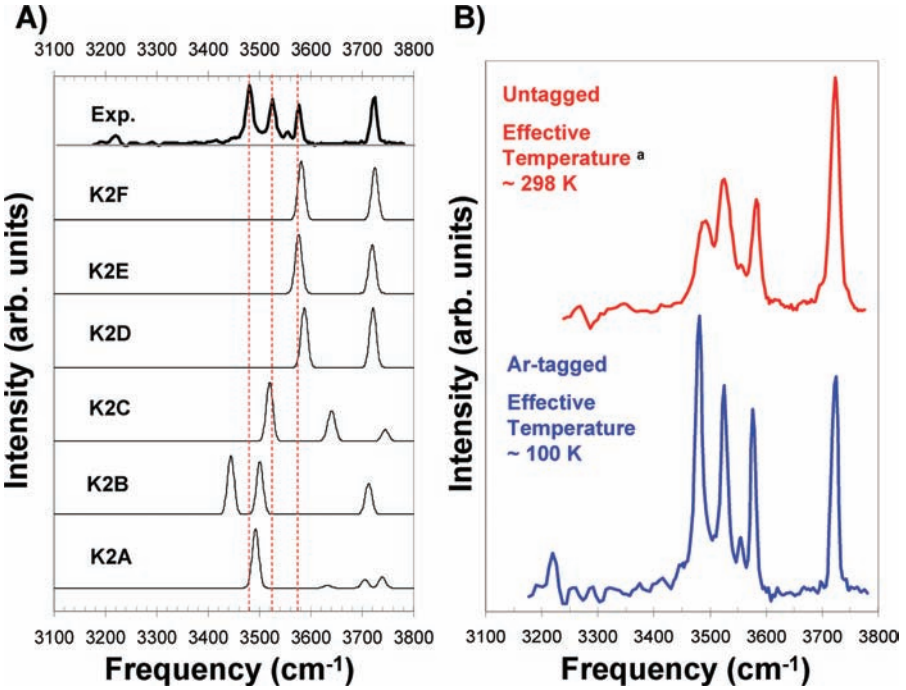

Figure 9. (A) Comparison between experiment and calculations for $K^+(18c6)(H_2O)_2$. (B) Temperature dependent spectra for $K^+(18c6)(H_2O)_2$. [a]The untagged spectra have been previously reported in ref 17. All of the spectra have been normalized to their maximum intensity and offset for clarity. The red-dotted line in (A) is used to guide the eye and facilitate comparison with the simulated spectra.

Like the $Na^+(18c6)(H_2O)_2Ar$ system, the $K^+(18c6)(H_2O)_2Ar$ system also offers the opportunity to gauge the temperature dependence of the spectra when comparing Ar-tagged and untagged species. As in the Na^+ case shown in Figure 8B, the untagged and Ar-tagged spectra of $K^+(18c6)(H_2O)_2$ are shown in Figure 9B. While the difference between the spectra of the tagged and untagged species is not as pronounced in the $K^+(18c6)(H_2O)_2$ system as it was for the $Na^+(18c6)(H_2O)_2$ system, there are differences in the relative intensity of the hydrogen-bonded OH stretches. In particular, the middle feature at 3525 cm^{-1} is the

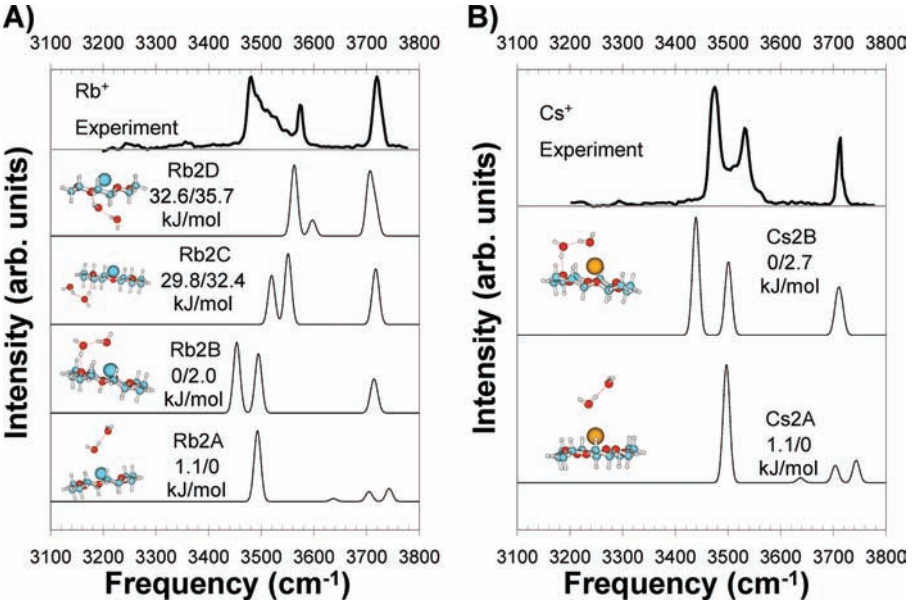

Figure 10. Comparison of experimental IRPD spectra and simulated IR spectra for each candidate geometry shown for the (A) $Rb^+(18c6)(H_2O)_2$ and (B) $Cs^+(18c6)(H_2O)_2$ systems. All of the spectra have been normalized to their maximum intensity and offset for clarity. The relative Gibbs free energies (ΔG in kJ/mol) are also given at 0 K/100 K.

dominant feature in the spectrum of the warm species. This is not the case in the spectrum of the colder species and is likely due to a clear energetic preference[17] for conformer K2A over K2B by 10.3 kJ/mol at 298 K, and the absence of Ar from influencing the relative stabilities.

For the Rb^+ and Cs^+ systems, we shall examine only the conformers that are most likely present in the experiment and include all others in the Supporting Information. The candidate conformers and their simulated IR spectra and relative energies are shown along with the experimental spectra for $Rb^+(18c6)(H_2O)_2$ and $Cs^+(18c6)(H_2O)_2$ in Figure 10. The two lowest-energy conformers shown for each ion feature the waters in same-side binding configurations. This configuration allows both the waters and 18c6 to interact with the ion. This is not too surprising since Rb^+ and Cs^+ are too large to bind via sandwich-type configurations without a large energetic cost. There is a significant broadening in the $Rb^+(18c6)(H_2O)_2$ experimental spectrum compared to the $K^+(18c6)(H_2O)_2Ar$ spectrum, although the overall profile is very similar. The broadening is likely due to multiple conformers, with overlapping hydrogen-bonded OH stretches, being sampled in the experiment. We cannot rule out the presence of any of the conformers shown for Rb^+ based on their simulated IR spectra. Conformer Rb2B replicates the region between ~3460 and 3520 cm^{-1} well, while Rb2D is excellent at replicating the region just below ~3600 cm^{-1} as well as the free OH region. The $Cs^+(18c6)(H_2O)_2Ar$ experimental spectrum is shown with the simulated IR spectrum for Cs2A and Cs2B in Figure 10B. Conformer Cs2B does a remarkable job at replicating the overall profile of the experimental spectrum. This conformer features both $H_2O\cdots H_2O$ and $18c6\cdots H_2O$ hydrogen bonding, with the former type giving rise to the lower frequency hydrogen-bonded OH stretch in the experimental spectrum at ~3476 cm^{-1} and the latter type of interaction responsible for the weaker hydrogen-bonded OH stretch at ~3534 cm^{-1}. While Rb2A and Cs2A conformers are slightly lower in energy (but within our uncertainty), conformers

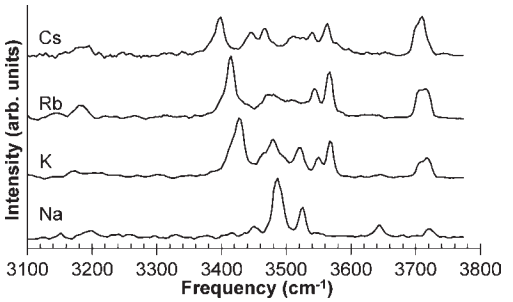

Figure 11. Experimental IRPD spectral summary of $M^+(18c6)(H_2O)_3Ar$ complexes in the OH stretching region monitoring the loss of Ar.

Rb2B and Cs2B once again facilitate a direct $Ar\cdots M^+$ interaction, which favors the latter two conformers.

3.3. $M^+(18c6)(H_2O)_3Ar$ Complexes. The experimental spectra for $M^+(18c6)(H_2O)_3Ar$ systems monitoring the loss of Ar are shown in Figure 11. Starting with $n = 3$, we were unable to make Ar-tagged Li^+ complexes in sufficient numbers for spectroscopic experiments. However, as was the case for the smaller complexes, there is still a distinction between the spectra for Na^+ and the larger ions, starting with K^+ (vide infra). Among of the most noticeable aspects of Figure 11 are the resolvable features present in the hydrogen-bonded OH stretching region of the spectra even with three waters present. This was not the case for the warm, untagged species[17] and illustrates the spectroscopic advantage of using Ar-tagging. Since there are a large number of low-lying conformations found for all of the $n = 3$ complexes, we discuss only the few in this section that are likely populated in our experiment. The rest are contained in the Supporting Information.

The $Na^+(18c6)(H_2O)_3Ar$ spectrum shown in Figure 11 is strikingly simple, and clearly distinguishable from the larger alkali metal ions. As shown in Figure 12, this is because only the global-minimum configuration, a 2/1 sandwich configuration featuring

two waters above the 18c6 on the same side as Na^+ and one below 18c6, seems to be sampled in our experiment. This conformer is favored by 4.1 kJ/mol at 100 K over the next lowest conformer. The overall profile of the simulated IR spectrum and the experiment correlate fairly well and the binding motif is similar to several conformers shown in Figure 6, including Na2A. There are two sharp hydrogen-bonded OH stretches in the experimental spectrum at 3487 and 3525 cm^{-1}. The 3487 cm^{-1} feature is due to the $O-H\cdots O_{18c6}$ hydrogen bond of the bottom H_2O. This H_2O also gives rise to the free OH present at 3721 cm^{-1}. The double-donor H_2O on the top side gives rise to two features in the experimental spectrum, a symmetric and asymmetric stretch. The symmetric stretch is located at 3525 cm^{-1} and is shifted by 135 cm^{-1} to lower-frequency relative to the symmetric stretch of gas-phase neutral[48] H_2O. The asymmetric vibration is present at 3645 cm^{-1} in the experiment, and is shifted by 111 cm^{-1} relative to gas-phase neutral[48] H_2O. We are not adequately able to resolve the symmetric and asymmetric vibrations of the top H_2O, which is a single-acceptor-type H_2O in the experimental spectrum.

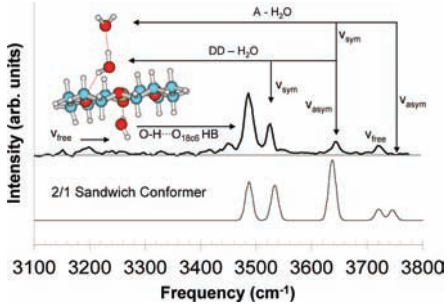

Figure 12. Despite its relatively large size, there appears to be a single dominant conformer (2/1 sandwich-type) present in the experiment for $Na^+(18c6)(H_2O)_3Ar$. The peak assignments for the experimental (top) spectrum are shown. Both of the spectra have been normalized to their maximum intensity and offset for clarity.

The spectra involving the larger alkali ions in Figure 11 are more complex than for $Na^+(18c6)(H_2O)_3Ar$, reflecting the presence of multiple conformers. With three waters present in the cluster, there are only two different possibilities for H_2O configurations around the 18c6-M^+ complex, which are three waters in a same-side configuration or a 2/1 sandwich-type configuration, with two waters on one side and one on the other side. The same-side conformers that we include in Figure 13 for K^+, Rb^+, and Cs^+ are the linear trimer, cyclic trimer (not a stable conformer for K^+), 1+2 trimer, and 2+1 trimer. For the latter two types, the first number refers to the number of waters directly interacting with the ion (i.e., first-shell-type waters). In addition to the 2/1 sandwich conformer we also consider a modified sandwich conformer (H 2/1 sand), where the two waters on the same side are forming $H_2O\cdots H_2O$ and $18c6\cdots H_2O$ hydrogen bonds. The energies shown for each conformer are relative to the lowest energy conformer at 100 K which is the linear trimer for all cases.

In contrast to Na^+, complexes with the larger ions have additional features to both lower and higher frequency in the hydrogen-bonded OH stretching region (3400 to 3600 cm^{-1}) as can be seen in Figure 11. From the calculated spectra in Figure 13, the linear hydrogen-bonded H_2O trimer chain (the global minimum structure for K^+, Rb^+ and Cs^+), specifically the hydrogen-bonded OH on H_2O bound to the ion, consistently provides a strong IR feature near 3400 cm^{-1}. This is in agreement with the experimental spectra shown in Figures 11 and 13. To the high frequency side, near 3560 cm^{-1}, there is a persistent doublet for all of the larger alkali metal ions. From the calculations, the 2 + 1 trimer appears to come closest to replicating the splitting in the experimental spectra. This conformation has previously been detected[27] in the $Cs^+(H_2O)_nAr$ system. It is also interesting to note that there is a connection between the Na^+ and K^+ spectra,

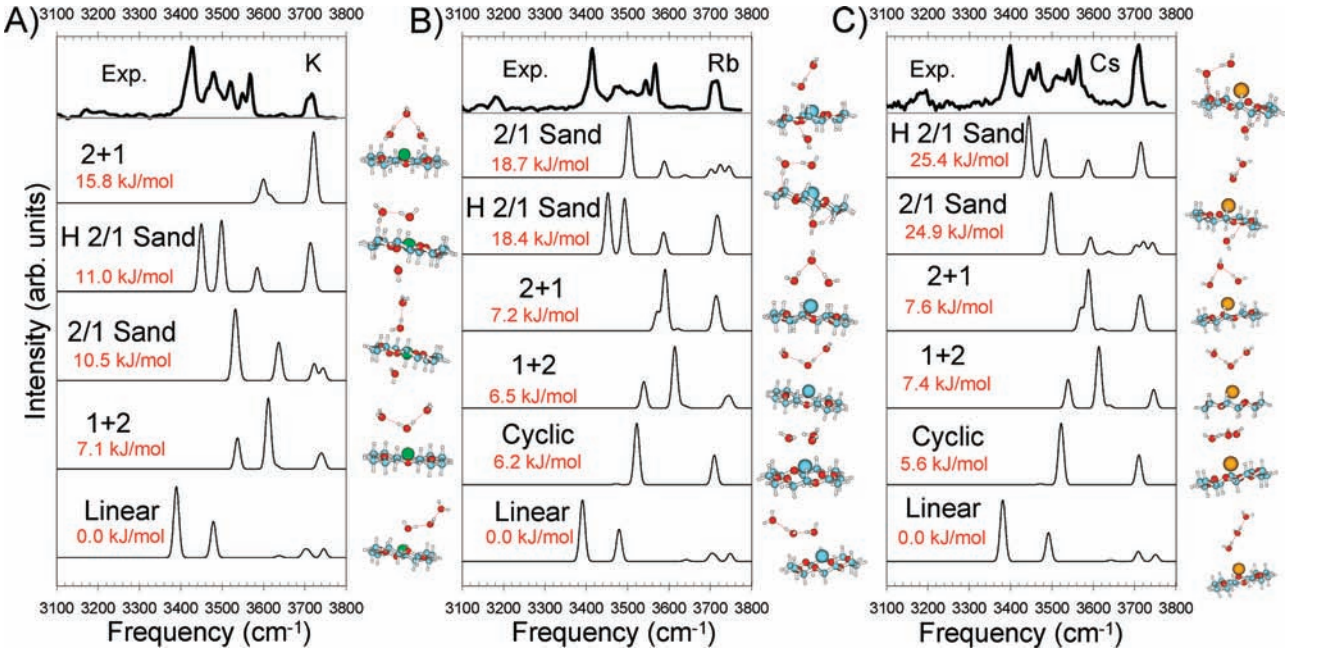

Figure 13. Comparison of experiment with calculations for selected $M^+(18c6)(H_2O)_3$ conformers, for M = (A) K, (B) Rb, and (C) Cs. The relative Gibbs free energies (ΔG in kJ/mol) are given at 100 K. The conformers are ordered according to their 100 K energies. The geometries are based on the B3LYP/6-31+G** level of theory. All of the spectra have been normalized to their maximum intensity and offset for clarity.

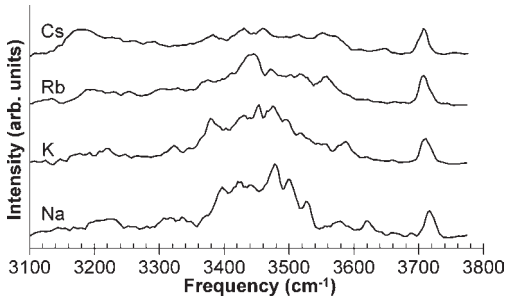

Figure 14. Experimental IRPD spectral summary of $M^+(18c6)(H_2O)_4Ar$ complexes in the OH stretching region monitoring the loss of Ar.

as seen in Figure 11. The pronounced doublet at ~3478 and 3519 cm^{-1} provides support for the presence of a common sandwich-type conformer, possibly the 2/1 sandwich-type, among those present for K^+. The H 2/1 sandwich-type conformer also cannot be ruled out for K^+ since it is essentially isoenergetic to the 2/1 sandwich-type conformer and may actually give rise to some of the breadth to the bands between ~3450−3550 cm^{-1} in the $K^+(18c6)(H_2O)_3Ar$ spectrum compared to the $Na^+(18c6)(H_2O)_3Ar$ spectrum (Figure 11). The existence of this conformer is not likely for Na^+ since the 2/1 sandwich conformer is favored over the H 2/1 sandwich conformer by 7.3 kJ/mol at 100 K and there is good agreement between the experimental and the 2/1 sandwich configuration simulated spectrum (Figure 12).

The $M^+(18c6)(H_2O)_3Ar$ cluster ions show an extremely insightful view to the competition between the various noncovalent interactions. For Na^+, with an ionic radius slightly too small to sit optimally inside the cavity of 18c6, the 18c6 and H_2O oxygens strongly compete to coordinate with the Na^+. This results in the sandwich-type structure, with waters above and below the plane of 18c6, being the favored configuration. With K^+, there is an optimal fit between the ion and the 18c6, substantially reducing the availability of the ion to H_2O molecules. As a result, the most energetically favored configurations have the all the H_2O molecules on one side of the crown ether (the linear and 1+2 conformers in Figure 13A). Sandwich structures are now higher in energy but appear to make contributions to the experimental spectrum. For Rb^+ and Cs^+, the ions are too large for the 18c6 cavity and sit just above the plane of the crown ether. This makes the ions more available for $H_2O\cdots M^+$ interactions and the four lowest energy conformers for each ion have the three waters on the same side of the crown ether as the ion (linear, cyclic, 1+2, and 2+1 as shown in Figure 13B and 13C). Water−water interactions have reached the point where the cyclic water trimer structure (the global minimum structure for neutral H_2O trimer) is the second lowest energy conformer. This indicates that the $H_2O\cdots M^+$ interaction (maximizing the number of ion−water contacts), is again effectively competing against the interaction between the ion and the etheric oxygens. The sandwich configurations are much higher in energy.

3.4. $M^+(18c6)(H_2O)_4Ar$ Complexes. The experimental spectra for $M^+(18c6)(H_2O)_4Ar$ systems monitoring the loss of Ar are shown in Figure 14. The spectra contain only broad features which preclude comparison with our DFT calculations, although we include the complete summary of our calculations for $M^+(18c6)(H_2O)_4Ar$ systems in the Supporting Information. In contrast to the $n = 1-3$ systems, there is no longer a clear distinction between the spectra of the smaller (Na^+) and larger ions. This could be due to many reasons, perhaps the most likely being the size and spectral breadth arising from multiple conformers. This indicates that at least for these systems, there is a size limit to the use of Ar-tagging for generating resolvable spectra. It is important to note that the binding energy of H_2O in these cluster ions has lowered to the point where the loss of Ar + H_2O, (and not the loss of Ar) is the preferred loss channel in terms of energy balance, i.e. the energy of the photon is best matched by the energy loss associated with dissociation of both H_2O and Ar. We include the spectra acquired monitoring the loss of Ar + H_2O in the Supporting Information. Like the spectra acquired monitoring the loss of Ar, the broad nature of the features precludes individual conformer assignment.

4. CONCLUSIONS

In an earlier study[18] dealing with the Ar-tagged dehydrated $M^+(12c4)$ and $M^+(18c6)$ systems, we were unable to observe a specific behavior that could be assigned to the $Li^+(12c4)$ or $K^+(18c6)$ systems. While the negative finding suggested that there might not be a spectroscopic signature for selectivity in the gas phase, the findings of this study along with the complementary warm[17] $M^+(18c6)(H_2O)_{1-4}$ study indicates that microhydration must be included to observe unique trends. In both the untagged study[17] and this Ar-tagged study the most important finding is not a single spectroscopic signature of selectivity, but rather the unique configurations by systems containing K^+ in contrast to both smaller and larger ions. Since K^+ has the "best fit" with 18c6, the $18c6\cdots K^+$ interaction dominates, weakening the ability of the ion to interact with H_2O. This favors one point of contact between the H_2O and the ion. Unique binding for K^+ has also been noted in a previous gas-phase study by Bowers and coworkers[49] of the alkali metal ions with 18c6. In the present study, there are a number of effects that are associated with the special role of K^+. Perhaps the most notable is a significant difference in the spectra between the smaller ions, Li^+ and Na^+, and K^+ for $M^+(18c6)(H_2O)_{1-3}Ar$. This is due to the smaller size of the ions fostering strong $18c6\cdots M^+$, $H_2O\cdots M^+$, and $18c6\cdots H_2O$ interactions. Experimentally, the combination of these interactions leads to lower frequency hydrogen-bonded OH stretching modes for these two ions in comparison to K^+. Our computational results also support this picture and indicate that the smaller ions are not successfully sequestered by 18c6, and H_2O molecules readily interact both with the 18c6 and the ion on either side of 18c6 via sandwich-type conformations. This is likely due to the limited flexibility of the 18c6, preventing maximal interaction between the smaller ions and the six etheric oxygens.

The larger ions, Rb^+ and Cs^+, are positioned sufficiently above the plane of 18c6, so that the $H_2O\cdots M^+$ interaction becomes very competitive, with multiple H_2O molecules interacting with the ion (as clearly seen in the cyclic and 2+1 trimer structures in Figure 13). This reflects the freedom of H_2O to migrate and optimize its interactions with the larger alkali ions. All of these trends are a result of the optimum relationship between the size of K^+ and the 18c6 cavity. This special relationship allows for the unique balance of $18c6\cdots M^+$, $18c6\cdots H_2O$, and $M^+\cdots H_2O$ interactions. In all cases, however this spectral distinction weakens with increasing hydration as $H_2O\cdots H_2O$ hydrogen-bonding interactions become increasingly important. This limit is seen

in the $n = 4$ spectra, where there are only slight changes in the spectra regardless of ion size.

■ ASSOCIATED CONTENT

Supporting Information. Complete refs 32 and 33, along with additional results. This material is available free of charge via the Internet at http://pubs.acs.org.

■ AUTHOR INFORMATION

Corresponding Author
j-lisy@uiuc.edu

■ ACKNOWLEDGMENT

The authors thank the National Science Foundation (Grants CHE-0748874 and CRIF-0541659) for partial support of this research. Computational work was done on NCSA Cobalt Supercomputer System (Award no. TG-CHE070097) and Abe Supercomputer System (Award no. TG-CHE100063). The authors also acknowledge useful comments by the reviewers that assisted in improving the overall agreement between the experimental and computational results.

■ REFERENCES

(1) Pedersen, C. J. *J. Am. Chem. Soc.* **1967**, *89*, 2495–2496.
(2) Pedersen, C. J. *J. Am. Chem. Soc.* **1967**, *89*, 7017–7036.
(3) Izatt, R. M. *Chem. Soc. Rev.* **2007**, *36*, 143–147.
(4) Pedersen, C. J.; Frensdorff, H. K. *Angew. Chem., Int. Ed.* **1972**, *11*, 16–25.
(5) Izatt, R. M.; Rytting, J. H.; Nelson, D. P.; Haymore, B. L.; Christensen, J. J. *Science* **1969**, *164*, 443–444.
(6) Izatt, R. M.; Nelson, D. P.; Rytting, J. H.; Haymore, B. L.; Christensen, J. J. *J. Am. Chem. Soc.* **1971**, *93*, 1619–1623.
(7) Izatt, R. M.; Terry, R. E.; Nelson, D. P.; Chan, Y.; Eatough, D. J.; et al. *J. Am. Chem. Soc.* **1976**, *98*, 7626–7630.
(8) Zhang, H.; Chu, I. H.; Leming, S.; Dearden, D. V. *J. Am. Chem. Soc.* **1991**, *113*, 7415–7417.
(9) Dearden, D. V.; Zhang, H.; Chu, I. H.; Wong, P.; Chen, Q. *Pure Appl. Chem.* **1993**, *65*, 423–428.
(10) Maleknia, S.; Brodbelt, J. *J. Am. Chem. Soc.* **1992**, *114*, 4295–4298.
(11) Brodbelt, J. S.; Liou, C.-C. *Pure Appl. Chem.* **1993**, *65*, 409–414.
(12) More, M. B.; Ray, D.; Armentrout, P. B. *J. Am. Chem. Soc.* **1999**, *121*, 417–423.
(13) Armentrout, P. B. *Int. J. Mass Spectrom.* **1999**, *193*, 227–240.
(14) Feller, D. *J. Phys. Chem. A* **1997**, *101*, 2723–2731.
(15) Rodriguez, J. D.; Lisy, J. M. *Int. J. Mass Spectrom.* **2009**, *283*, 135–139.
(16) Rodriguez, J. D.; Lisy, J. M. *J. Phys. Chem. A* **2009**, *113*, 6462–6467.
(17) Rodriguez, J. D.; Vaden, T. D.; Lisy, J. M. *J. Am. Chem. Soc.* **2009**, *131*, 17277–17285.
(18) Rodriguez, J. D.; Kim, D.; Tarakeshwar, P.; Lisy, J. M. *J. Phys. Chem. A* **2010**, *114*, 1514–1520.
(19) Kusaka, R.; Inokuchi, Y.; Ebata, T. *Phys. Chem. Chem. Phys.* **2007**, *9*, 4452–4459.
(20) Kusaka, R.; Inokuchi, Y.; Ebata, T. *Phys. Chem. Chem. Phys.* **2008**, *10*, 6238–6244.
(21) Kusaka, R.; Inokuchi, Y.; Xantheas, S. S.; Ebata, T. *Sensors* **2010**, *10*, 3519–3548.
(22) Martinez-Haya, B.; Hurtado, P.; Hortal, A. R.; Steill, J. D.; Oomens, J.; et al. *J. Phys. Chem. A* **2009**, *113*, 7748–7752.
(23) Martinez-Haya, B.; Hurtado, P.; Hortal, A. R.; Hamad, S.; Steill, J. D.; et al. *J. Phys. Chem. A* **2010**, *114*, 7048–7054.
(24) Shubert, V. A.; James, W. H.; Zwier, T. S. *J. Phys. Chem. A* **2009**, *113*, 8055–8066.
(25) Choi, C. M.; Lee, J. H.; Choi, Y. H.; Kim, H. J.; Kim, N. J.; et al. *J. Phys. Chem. A* **2010**, *114*, 11167–11174.
(26) Robertson, W. H.; Johnson, M. A. *Annu. Rev. Phys. Chem.* **2003**, *54*, 173–213.
(27) Miller, D. J.; Lisy, J. M. *J. Am. Chem. Soc.* **2008**, *130*, 15381–15392.
(28) Nicely, A. L.; Miller, D. J.; Lisy, J. M. *J. Am. Chem. Soc.* **2009**, *131*, 6314–6315.
(29) Beck, J. P.; Lisy, J. M. *J. Phys. Chem. A* **2010**, *114*, 10011–10015.
(30) Beck, J. P.; Lisy, J. M. *J. Phys. Chem. A* **2011**, *115*, 4148–4156.
(31) Rodriguez, O.; Lisy, J. M. *J. Phys. Chem. Lett.* **2011**, *2*, 1444–1448.
(32) Deppmeier, B. J.; Driessen, A. J.; Hehre, T. S.; Hehre, W. J.; Johnson, J. A.; et al. *SPARTAN 2002*, SGI IRIX 64 (mips4) ed.; Irvine, CA, 2002.
(33) Frisch, M. J.; et al. *Gaussian03*, Revision B.04; Pittsburgh, PA, 2003.
(34) Hay, P. J.; Wadt, W. R. *J. Chem. Phys.* **1985**, *82*, 270–283.
(35) Wadt, W. R.; Hay, P. J. *J. Chem. Phys.* **1985**, *82*, 284–298.
(36) Hay, P. J.; Wadt, W. R. *J. Chem. Phys.* **1985**, *82*, 299–310.
(37) Glendening, E. D.; Feller, D.; Thompson, M. A. *J. Am. Chem. Soc.* **1994**, *116*, 10657–10669.
(38) Schaftenaar, G.; Noordik, J. H. *J. Comput.-Aided Mol. Design* **2000**, 123–134.
(39) Gorelsky, S. I. *CCRI*; University Of Ottawa, Canada, 2008.
(40) Bouteiller, Y.; Gillet, J.; Gregoire, G.; Schermann, J. P. *J. Phys. Chem. A* **2008**, *112*, 11656–11660.
(41) Irikura, K. K., National Institute of Standards and Technology, 2002.
(42) Maciej, K.; Han Myoung, L.; Young Cheol, C.; Kwang, S. K.; Tarakeshwar, P.; et al. *J. Chem. Phys.* **2007**, *126*, 074302.
(43) Vaden, T. D.; Weinheimer, C. J.; Lisy, J. M. *J. Chem. Phys.* **2004**, *121*, 3102–3107.
(44) Vaden, T. D.; Lisy, J. M.; Carnegie, P. D.; Dinesh Pillai, E.; Duncan, M. A. *Phys. Chem. Chem. Phys.* **2006**, *8*, 3078–3082.
(45) Nicely, A. L.; Miller, D. J.; Lisy, J. M. *J. Mol. Spectrosc.* **2009**, *257*, 157–163.
(46) Huisken, F.; Kaloudis, M.; Kulcke, A. *J. Chem. Phys.* **1996**, *104*, 17.
(47) Frensdorff, H. K. *J. Am. Chem. Soc.* **1971**, *93*, 600–606.
(48) Fraley, P. E.; Narahari Rao, K. *J. Mol. Spectrosc.* **1969**, *29*, 348–364.
(49) Lee, S.; Wyttenbach, T.; von Helden, G.; Bowers, M. T. *J. Am. Chem. Soc.* **1995**, *117*, 10159–10160.